Resonant photoionization cross sections and branching ratios for atomic oxygen

S. S. Tayal
Department of Physics, Clark Atlanta University, Atlanta, Georgia 30314
(Received 29 August 2001; published 27 February 2002)

Total and partial photoionization cross sections for the ejection of either a $2p$ or a $2s$ electron from the ground $2s^2 2p^4\ ^3P$ state of atomic oxygen have been investigated using the *R*-matrix method. Cross sections are dominated by Rydberg series of autoionizing resonances converging to several ionic states. The autoionizing states are analyzed and identified using a procedure of eigenphase gradients. Comparison of our results with available previous calculations and experiments is shown to lead to some interesting conclusions regarding the importance of electron correlation and normalization of the measured relative cross sections. Our calculation removed long-standing discrepancy between theory and experiment regarding the shape of photoionization cross section near the $^2P^o$ threshold. The calculated branching ratios for the production of $^4S^o$, $^2D^o$, and $^2P^o$ states at 584 and 304 Å show good agreement with experiments.

DOI: 10.1103/PhysRevA.65.032724 PACS number(s): 32.80.Fb

I. INTRODUCTION

The autoionizing resonances in the photoionization of the ground-state atomic oxygen have been studied by several theoretical and experimental research groups [1–24]. These studies have emphasized the importance of electron-correlation and interchannel coupling effects in atomic oxygen. The resonance structures in total and partial photoionization cross sections are mostly due to autoionizing Rydberg series converging to the $2s^2 2p^3\ ^2D^o$, $^2P^o$, $2s2p^4\ ^4P$, ^2D, ^2S, and ^2P ionic thresholds between 13.62 and 39.98 eV. These ionic states arise in the photoionization process leading to a removal of $2p$ or $2s$ electron from the initial ground $2s^2 2p^4\ ^3P$ state of atomic oxygen. The Rydberg series $2s^2 2p^3(^2D^o)ns\ ^3D^0$, $2s^2 2p^3(^2D^0)nd\ ^3S^0$, $^3D^o$ converge to the $^2D^o$ threshold, the $2s^2 2p^3(^2P^o)ns\ ^3P^o$, $2s^2 2p^3(^2P^o)nd\ ^3P^o$, $^3D^o$ converge to the $^2P^o$ ionic threshold, and $2s2p^4(^4P)np\ ^3S^o$, $^3P^o$, $^3D^o$ converge to the ^4P threshold. Various theoretical calculations and experiments show significant differences with each other in this energy region. In addition to intrinsic physical interest, photoionization cross sections of oxygen are important in the study of atmospheric processes in earth's upper atmosphere and planetary and stellar atmospheres owing to the abundance of oxygen.

Theoretical calculations have been performed in the close-coupling [1–5], random-phase approximation with exchange (RPAE) [6,7], Hartree-Fock (HF) [8], and *R*-matrix [9–11] approaches. The close-coupling theory was used by Henry [1,2], Smith [3], and Pradhan [4,5] to calculate photoionization parameters in atomic oxygen. Henry included $O^+\ ^4S^o$, $^2D^o$, and $^2P^o$ states in the close-coupling expansion and analyzed autoionizing resonances converging to the $O^+\ ^2D^o$ and $^2P^o$ thresholds. Smith considered five O^+ states ($2s^2 2p^3\ ^4S^o$, $^2D^o$, $^2P^o$, $2s2p^4\ ^4P$, ^2P) and presented partial cross sections and asymmetry parameters for leaving the O^+ ion in these states. Pradhan included $2s^2 2p^3\ ^4S^o$, $^2D^o$, $^2P^o$, $2s2p^4\ ^4P$, ^2P, ^2D, and ^2S ionic target states in the close-coupling expansion to calculate total and partial photoionization cross sections of oxygen. Pradhan reported branching ratios at 584 and 304 Å. The generalized RPAE [6,7] has also been used to calculate photoionization cross sections and asymmetry parameters of atomic oxygen. Taylor and Burke [9] carried out *R*-matrix calculation for the photoionization of the ground-state atomic oxygen by including eight O^+ states ($2s^2 2p^3\ ^4S^o$, $^2D^o$, $^2P^o$, $2s2p^4\ ^4P$, ^2P, ^2D, ^2S, $2s2p^5\ ^2P^o$) in the expansion. They analyzed the autoionizing resonances below the $^2D^o$, $^2P^o$, and ^4P thresholds. Bell *et al.* [10] also used *R*-matrix method to calculate total photoionization cross sections of the ground $2s^2 2p^4\ ^3P$ and excited $2s^2 2p^4\ ^1D$ and ^1S states of atomic oxygen. They included 11 O^+ states ($2s^2 2p^3\ ^4S^o$, $^2D^o$, $^2P^o$, $2s2p^4\ ^4P$, ^2P, ^2D, ^2S, $2s^2 2p^2 3s\ ^4P$, ^2P, ^2D, ^2S) in the *R*-matrix expansion. They represented target states by configuration-interaction (CI) wave functions obtained with the $1s$, $2s$, $2p$, $3s$, $3p$, and $3d$ orbitals. The eigenchannel *R*-matrix method has been used by Chen and Robicheaux [11] to calculate total photoionization cross section of the ground state.

On the experimental side, Huffman *et al.* [12] used a photographic technique to observe autoionizing states converging to the $^2D^o$ and $^2P^o$ thresholds. Kohl *et al.* [13] measured total photoionization cross section of oxygen in a limited energy region near the $^4S^o$ threshold using the dissociation produced in a shock heated gas. The technique of mass-resolved ion detection was used by Dehmer *et al.* [14,15], Samson and Pareek [16], and Angel and Samson [17] to measure total photoionization cross section. Samson and Pareek measured cross section in the wavelength range from 834 to 120 Å. Angel and Samson remeasured the cross section and extended the wavelength range to 44.3–910.5 Å. Angel and Samson used the calibaration scale of Samson and Pareek to place their measured relative cross section on an absolute scale. Dehmer *et al.* [15] reported relative cross section and observed autoionizing states below the $^2P^o$ threshold. The photoelectron spectroscopy (PES) technique was used by Hussein *et al.* [18], Dehmer and Dehmer [19], Samson and Petrosky [20], Samson and Hancock [21], and van der Meulen *et al.* [22,23] to measure partial cross sections and branching ratios for leaving the O^+ ion in the $^4S^o$, $^2D^o$, and $^2P^o$ states. Samson and Hancock measured branching ratios at 736 and 584 Å and Dehmer and Dehmer at 580 Å.

TABLE I. Parameters of the radial functions used in the calculation.

Orbital	Powers of r	Exp.	Coeff.	Orbital	Powers of r	Exp.	Coeff.
$3s$	1	6.892 71	0.108 98	$4p$	2	2.347 94	0.877 50
	2	2.372 02	−0.376 67		3	1.377 51	−2.436 54
	3	4.114 27	−0.080 20		3	1.578 60	0.127 43
	3	1.062 44	1.075 08		4	1.125 02	1.776 90
					4	1.181 59	0.131 19
$4s$	1	6.128 90	0.119 64	$3d$	3	1.993 24	0.106 49
	2	2.419 84	−0.519 78		3	0.708 63	0.951 83
	3	1.313 65	1.101 72	$4d$	3	2.196 31	4.697 79
	4	0.773 54	−1.216 67		4	2.491 82	−4.215 86
$3p$	2	4.856 54	0.143 06	$4f$	4	3.365 43	1.0000
	3	3.545 66	0.285 85				
	4	0.984 23	−1.004 21				

Hussein *et al.* measured partial cross sections for the production of the O^+ $^4S^o$, $^2D^o$, and $^2P^o$ states in the wavelength region between 725 and 580 Å. Van der Meulen *et al.* measured relative partial photoionization cross sections for leaving the O^+ ion in the $^4S^o$ and $^2D^o$ states in the energy region from the $^4S^o$ threshold at 13.62 eV to 30 eV. They focused on autoionizing Rydberg states below the $^2D^o$, $^2P^o$, and ^4P thresholds. They placed their results on an absolute scale using the cross section of van der Meer *et al.* [24]. The measured cross sections from the two most recent experiments of Angel and Samson [17] and van der Meulen *et al.* [23] show significant differences. Most of the differences in the two experiments seem to be caused by calibaration standards to arrive at absolute cross sections. Based on a sum-rules analysis, Berkowitz [25] argued that the calibaration of van der Meulen *et al.* may be in error. Seaton [26] presented a review and compilation of the available earlier theoretical and experimental photoionization results for oxygen.

In view of the lack of accurate theoretical calculation of partial cross sections or branching ratios for leaving the O^+ ion in various final ionic states in the photoionization of oxygen, we have performed a fairly extensive *R*-matrix calculation to obtain partial photoionization cross sections across autoionizing series of resonances. The initial O ($2s^22p^4\,^3P$) state, the final O^+ plus photoelectron ($^3S^o$, $^3P^o$, $^3D^o$) states, and the residual O^+ [$2s^22p^3\,^4S^o$, $^2D^o$, $^2P^o$, $2s2p^4\,^4P$, ^2D, ^2P, ^2S, $2s^22p^23s\,^4P$, ^2P, $2s^22p^23p\,^4D^o$, $^4P^o$, $^4S^o$, $^2D^o$, $^2P^o$, $^2S^o$, $2s^22p^23s'\,^2D$, $2s^22p^23p'\,^2F^o$, $^2D^o$, $2s^22p^23s''\,^2S$; where $3s'$ and $3p'$ represent $2p^2(^1D)$ core and $3s''$ represents $2p^2(^1S)$ core] states are represented by CI wave functions. The autoionizing Rydberg series of resonances below the O^+ $^2D^o$, $^2P^o$, and ^4P thresholds are analyzed. The positions E_r, effective quantum numbers n^*, and widths Γ_r of the major resonances of the $2s^22p^3(^2D^o)nl$ ($l=0,2$), $2s^22p^3(^2P^o)nl$ ($l=0,2$), and $2s2p^4(^4P)np$ Rydberg series are reported. The photoelectron angular distribution asymmetry parameters for leaving the O^+ ion in the $^4S^o$, $^2D^o$, and $^2P^o$ states have been recently reported [27].

II. COMPUTATIONAL DETAILS

We calculated partial and total photoionization cross sections for the $2p$ and $2s$ subshells of the ground $2s^22p^4\,^3P$ state of atomic oxygen in both length and velocity formulations. The $^3S^o$, $^3P^o$, and $^3D^o$ final states are allowed by dipole selection rules in LS coupling. Each of the 19 O^+ ionic states included in our calculation is described by CI wave functions constructed from ten orthogonal one-electron orbitals: $1s$, $2s$, $2p$, $3s$, $3p$, $3d$, $4s$, $4p$, $4d$, and $4f$. The $1s$, $2s$, and $2p$ radial functions are those given by Clementi and Roetti [28] and $3s$, $3p$, $3d$, $4s$, $4p$, $4d$, and $4f$ radial functions are obtained using the structure code CIV3 [29]. The $3s$, $3p$, and $3d$ orbitals are spectroscopic and are

TABLE II. Calculated and experimental ionization energies (eV).

State	Present	Expt.
$2s^22p^3\,^4S^o$	13.505	13.618
$2s^22p^3\,^2D^o$	16.841	16.943
$2s^22p^3\,^2P^o$	18.548	18.635
$2s2p^4\,^4P$	28.337	28.488
$2s2p^4\,^2D$	34.089	34.198
$2s^22p^23s\,^4P$	36.376	36.605
$2s^22p^23s\,^2P$	36.874	37.052
$2s2p^4\,^2S$	37.971	37.883
$2s^22p^23p\,^2S^o$	38.741	38.904
$2s^22p^23p\,^4D^o$	39.090	39.270
$2s^22p^23s'\,^2D$	39.243	39.279
$2s^22p^23p\,^4P^o$	39.294	39.460
$2s^22p^23p\,^2D^o$	39.761	39.858
$2s^22p^23p\,^4S^o$	39.838	39.923
$2s2p^4\,^2P$	40.048	39.983
$2s^22p^23p\,^2P^o$	40.478	40.165
$2s^22p^23p'\,^2F^o$	42.129	41.978
$2s^22p^23p'\,^2D^o$	42.344	42.129
$2s^22p^23s''\,^2S$	42.699	42.210

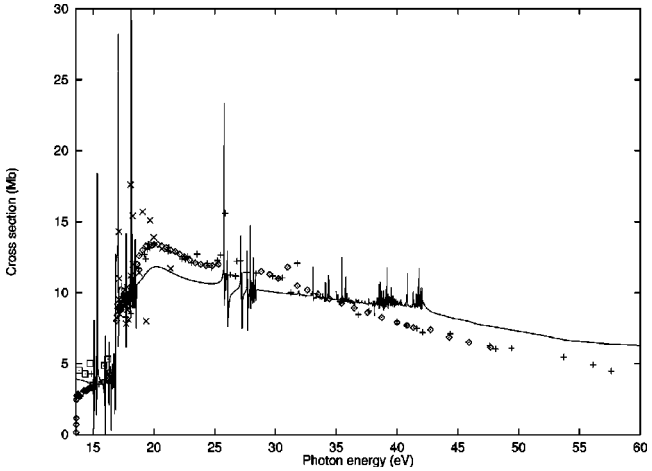

FIG. 1. Total photoionization cross section as a function of photon energy from the $^4S^o$ threshold to 60 eV. Solid curve, present cross section; diamonds, measured values of Angel and Samson (Ref. [17]); pluses, Samson and Pareek (Ref. [16]); rectangles, Kohl *et al.* (Ref. [13]); crosses, Hussein *et al.* (Ref. [18]).

optimized on the $2s^22p^23s\,^4P$, $2s^22p^23p\,^4P^o$, and $2s^22p^23d\,^4P$ states, respectively. The $4s$, $4p$, $4d$, and $4f$ are correlation functions and are chosen to improve the energies of ionic thresholds and the atomic oxygen ground state. The parameters of the orbitals are given in Table I. To account for electron correlation in ionic states, we used a total of 654 configurations to represent 19 states. The calculated ionization energies relative to the ground state of atomic oxygen are presented in Table II, where they are compared with the experimental values [30]. There is good agreement between the calculated and measured values.

The initial $2s^22p^4\,^3P$ bound state and the final O^+ ion plus photoelectron states are represented by the same types of *R*-matrix expansions. The initial state is described as a bound state of the electron plus O^+ ion system. The total wave function is expanded in an internal region surrounding the atom as [31]

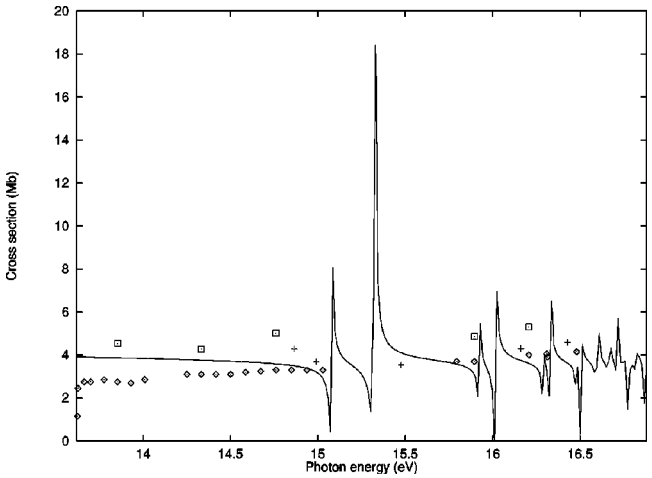

FIG. 2. Total photoionization cross section as a function of photon energy between the $^4S^o$ and $^2D^o$ thresholds. Notations are the same as in Fig. 1.

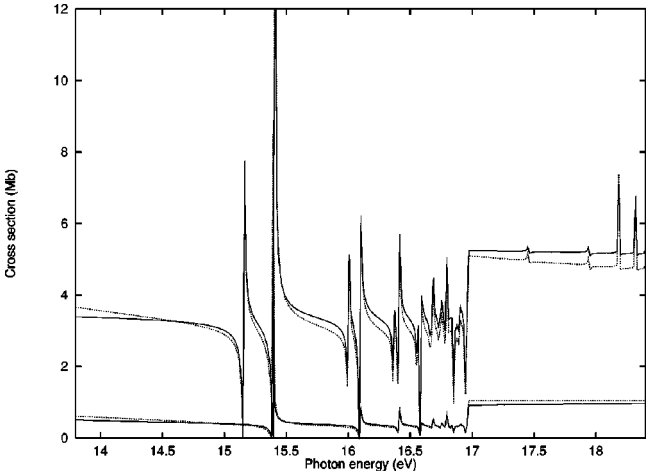

FIG. 3. Partial cross section as a function of photon energy between the $^4S^o$ and $^2P^o$ thresholds. Upper solid and dotted curves, present length and velocity cross sections, respectively, for the $^3D^o$ final state. Lower solid and dotted curves, present length and velocity cross sections, respectively, for the $^3S^o$ final state.

$$\Psi_k = A\sum_{ij} a_{ijk}\bar{\Phi}_i u_j(r) + \sum_j b_{jk}\phi_j, \qquad (1)$$

where $\bar{\Phi}_i$ are channel functions formed from he multiconfigurational functions of the O^+ target states and u_j are the numerical basis functions for the photoelectron. The operator A antisymmetrizes the wave function and a_{ijk} and b_{jk} are expansion coefficients determined by diagonalizing the $(N+1)$-electron Hamiltonian. The functions ϕ_j in Eq. (1) are of bound-state type and are included to compensate for the imposition of orthogonality conditions. Additional functions ϕ_j are included to allow for the short-range electron-

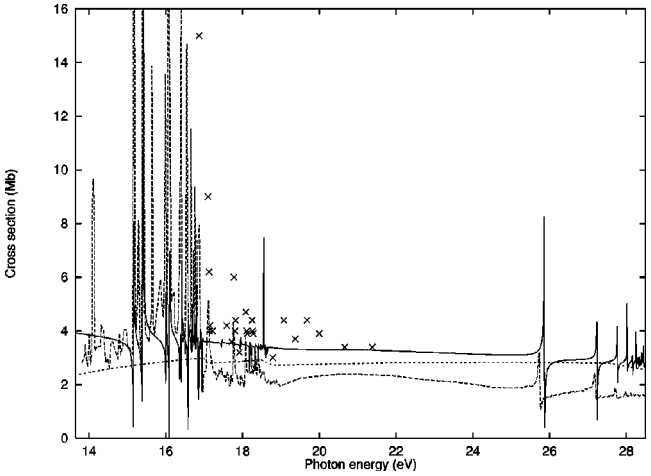

FIG. 4. Partial photoionization cross section for leaving the ion in the $^4S^o$ state as a function of photon energy between the $^4S^o$ and ^4P thresholds. Solid curve, present cross section; long-dashed curve, measured results of van der Meulen *et al.* (Ref. [23]); short-dashed curve, close-coupling results of Smith (Ref. [3]); crosses, measured values of Hussein *et al.* (Ref. [18]).

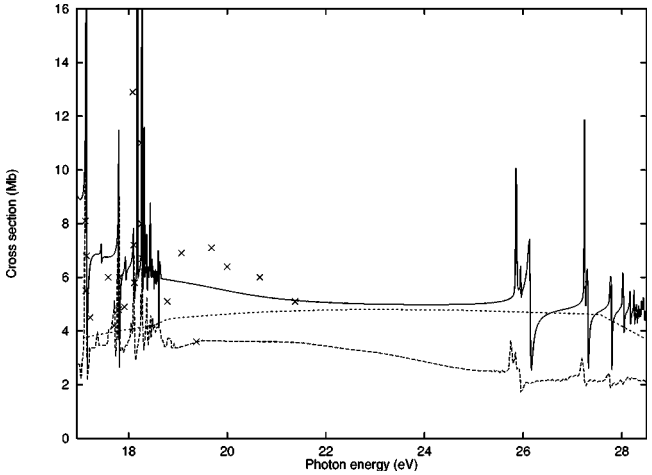

FIG. 5. Partial photoionization cross section for leaving the ion in the $^2D^o$ state as a function of photon energy between the $^2P^o$ and ^4P thresholds. Notations are the same as in Fig. 4.

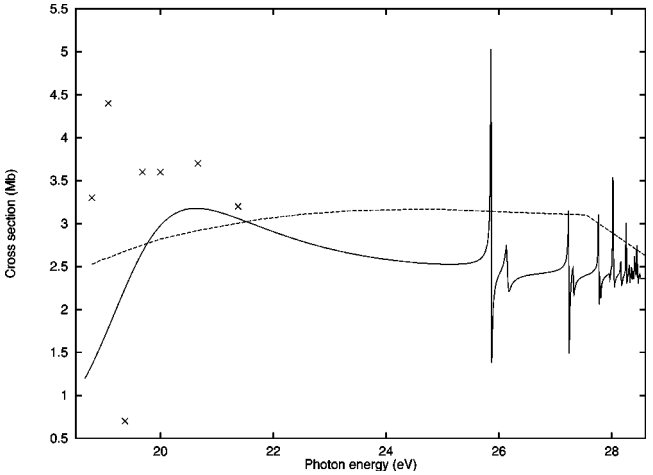

FIG. 6. Partial photoionization cross section for leaving the ion in the $^2P^o$ state as a function of photon energy between the $^2P^o$ and ^4P thresholds. Solid curve, present cross section; dashed curve, close-coupling calculation of Smith (Ref. [3]); crosses, measured results of Hussein *et al.* (Ref. [18]).

correlation effect. A boundary radius $r=20.55$ a.u. is introduced and 25 continuum orbitals in each channel are included.

III. RESULTS AND DISCUSSION

A. Total photoionization cross section

The total photoionization cross section is obtained by adding channel cross sections of all coupled channels for the $^3S^o$, $^3P^o$, and $^3D^o$ final states. The total photoionization cross section in the length formulation for photon energies from the $^4S^o$ threshold to 60 eV is displayed in Fig. 1. The measured cross sections of Angel and Samson [17], Samson and Pareek [16], Kohl *et al.* [13], and Hussein *et al.* [18] are also included in Fig. 1 for comparison. Most of the earlier theoretical work focused on total photoionization cross section of oxygen from the ground state. Our results agree well with the earlier *R*-matrix calculation of Bell *et al.* [10] (not shown) except for the structureless energy region above the $^2P^o$ threshold between 19–25 eV. The calculations of Bell *et al.* [10] and Pradhan [4] are in good agreement with each other, but show large discrepancies with the measurements of Angel and Samson [17] and Samson and Pareek [16] close to the $^4S^o$ threshold and above the $^2P^o$ threshold. The experimental results above the $^2P^o$ threshold exhibit an increasing trend and then a peak around 20 eV in contrast to these calculations that predicts a flat behavior of cross section in this energy region. Bell *et al.* speculated that the peak in the measured cross section may be related to the presence of molecular oxygen or atomic oxygen in excited states in the atomic beam. Our calculation agrees with the experimental data and predicts a broad peak in cross section above the $^2P^o$ threshold. The cause of the broad peak in cross sections is explained in the following section. The present total photoionization cross sections between the $^4S^o$ and $^2D^o$ thresholds are compared with the experimental results of Angel and Samson [17] and Kohl *et al.* [13] in Fig. 2. It is clear that our results are larger than those of Angel and Samson and smaller than the results of Kohl *et al.* in the photon energy region near the $^4S^o$ threshold. Our results differ by up to 50% with the experiment of Angel and Samson and agree with the calculation of Bell *et al.* in this energy region. Thus, the discrepancy above the $^2P^o$ threshold between the theory and experiment is now resolved, but there remains an unresolved discrepancy close to the $^4S^o$ threshold.

B. Partial cross sections

The partial cross sections in length and velocity forms for the $^3D^o$ and $^3S^o$ final states between the $^4S^o$ and $^2P^o$ ionic thresholds are shown in Fig. 3. The length and velocity forms of cross section differ normally by 5% to 7%. For the sake of clarity, we have plotted only length results of cross section in other figures. It can be seen from the Fig. 3 that the dominant

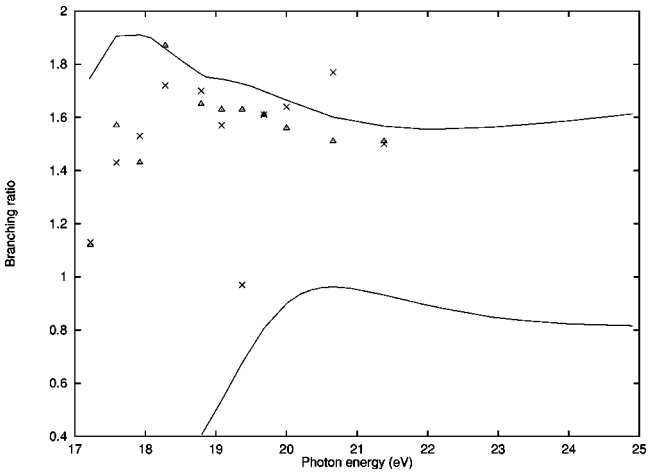

FIG. 7. Branching ratio as a function of photon energy between 17 and 25 eV. Branching ratio $\sigma(^2D^o)/\sigma(^4S^o)$: upper solid curve, present calculated ratio; open triangles, measured ratio of van der Meulen *et al.* (Ref. [23]); crosses, measured ratio of Hussein *et al.* (Ref. [18]). Branching ratio $\sigma(^2P^o)/\sigma(^4S^o)$: lower solid curve, present calculated ratio.

TABLE III. Comparison of present branching ratios with available other results.

Wavelength (Å)	$\frac{\sigma(^2D^o)}{\sigma(^4S^o)}$		$\frac{\sigma(^2P^o)}{\sigma(^4S^o)}$	
	Present	Others	Present	Others
584	1.57	1.57[a]; 1.29[b]; 1.48[c]; 1.57 ± 0.14[d]	0.94	0.85[a]; 0.81[b]; 0.95[c]; 0.82 ± 0.07[d]
304	1.81	1.34[a]; 1.18[b]; 1.49[c]; 1.64 ± 0.30[e]	1.05	0.86[a]; 1.34[b]; 0.99[c];

[a]Henry (Ref. [2]).
[b]Pradhan (Ref. [5]).
[c]Starace *et al.* (Ref. [8]).
[d]Samson and Petrosky (Ref. [20]).
[e]Dehmer and Dehmer (Ref. [19]).

contribution to the total cross section in this energy region is made by the $^3D^o$ final state. It may be noted that the series $2s^22p^3(^2D^o)nd\ ^3P^o$ has no continuum available below the $^2D^o$ threshold to autoionize in LS coupling.

The partial photoionization cross sections for leaving the ion in the $^4S^o$ state are shown in Fig. 4 together with the measured results of van der Meulen *et al.* [23] (long-dashed curve) and Hussein *et al.* [18] (crosses) and calculated values of Smith [3] (short-dashed curve) as a function of photon energy from the $^4S^o$ threshold to the $2s2p^4\,^4P$ threshold. Our background cross sections away from resonances are larger than the calculated nonresonant cross sections of Smith. The present calculated results are also larger than the experiment of van der Meulen *et al.*, particularly, above the $^2D^o$ threshold. The calculated $2s^22p^3(^2D^o)ns\ ^3D^o$ and $2s^22p^3(^2D^o)nd\ ^3S^o$ resonant states show excellent agreement with the experiment of van der Meulen *et al.*, except for the peak values of cross section that are larger in the experiment than in the theory. In addition to these resonances, the experiment also observed lower members $2s^22p^3(^2P^o)3s\ ^3P^o$ and $2s^22p^3(^2D^o)3d\ ^3P^o$ of the Rydberg series and the resonant state $2s2p^5\,^3P^o$ due to inner-shell excitation. These resonances are forbidden to autoionize in LS coupling. The resonance structure is weak between the $^2D^o$ and $^2P^o$ thresholds in both theory and experiment. Our results agree well with the experiment of Hussein *et al.* [18] except at energies close to the $^2P^o$ threshold. Our theory predicts well the position of the $2s2p^4(^4P)np\ ^3S^o$, $^3P^o$, and $^3D^o$ resonances and show good agreement with the experiment; the calculated resonance features slightly shifted to the higher energy. Only the lower members of the Rydberg series are resolved in the experiment.

The present partial photoionization cross sections for leaving the ion in the $^2D^o$ state are compared with the measured cross sections of van der Meulen *et al.* [23], Hussein *et al.* [18] and the close-coupling results of Smith [3] in Fig. 5. The position of major resonances from our theory and experiment of van der Meulen *et al.* seems to agree. However, the measured cross sections are lower than theory; a discrepancy perhaps caused by the normalization of the measured cross sections. There is a reasonable agreement with the experiment of Hussein *et al.* [18]. The partial cross section for leaving the ion in the $^2P^o$ state are shown in Fig. 6 together with the calculation of Smith [3] and experiment of Hussein *et al.* [18]. There are significant discrepancies between the two calculations for this case. The theoretical cross sections show large differences with the experiment of Hussein *et al.* These partial cross sections give rise to a broad peak in the total photoionization cross sections above the $^2P^o$ threshold. These are very sensitive to electron-correlation effects. The limited electron correlation may lead to flat cross section, as in the close-coupling calculation of Smith.

C. Branching ratios

The branching ratios $\sigma(^2D^o)/\sigma(^4S^o)$ and $\sigma(^2P^o)/\sigma(^4S^o)$ are shown in Fig. 7 as a function of photon energy. The present branching ratio $\sigma(^2D^o)/\sigma(^4S^o)$ (upper solid curve) is compared with the experimental value of van der Meulen *et al.* (triangles) and Hussein *et al.* (crosses). In the structureless region above 19 eV, our results agree very well in shape, but are larger in magnitude compared to the measured values of van der Meulen *et al.* Our partial cross section for leaving the ion in the $^4S^o$ state at 20 eV is about 40% larger than the experiment, while the present partial cross section for leaving the ion in the $^2D^o$ state at the same energy is about 52% larger. Though most of the discrepancies may have been caused by the normalization of experimental data, it seems that some of the discrepancies may be due to other systematic errors in the experiment. In the energy region below 19 eV, the branching ratio does not show smooth behavior because of the presence of autoionizing resonances. The experiment of Hussein *et al.* show large fluctuations in the branching ratio in the structureless energy region above 19 eV. The present branching ratios at 584 and 304 Å are compared with the available theoretical results of Henry [2], Pradhan [5], and Starace *et al.* [8] and the measured values of Samson and Petrosky [20] and Dehmer and Dehmer [19] in Table III. Our result for the $\sigma(^2D^o)/\sigma(^4S^o)$ ratio is in excellent agreement with the calculations of Henry and Sta-

TABLE IV. Resonance parameters of $2s^2 2p^3(^2D^o)ns,nd$ series converging to the $^2D^o$ threshold.

State	E_r (eV)	Γ_r (eV)	n^*	State	E_r (eV)	Γ_r (eV)	n^*
$4s\ ^3D^o$	15.148	4.37–4	3.742	$3d\ ^3D^0$	15.396	1.14–3	2.951
	15.274 [a]	8.82–5 [a]			15.410 [a]	4.36–4 [a]	
	15.229 [b]	9.30–5 [b]			15.420 [b]	3.89–4 [b]	
5*s*	15.994	1.76–4	4.757	4*d*	16.085	5.08–4	3.949
	16.026 [a]	4.23–5 [a]			16.079 [a]	2.88–4 [a]	
	16.000 [b]	4.34–5 [b]			16.080 [b]	2.59–4 [b]	
6*s*	16.358	8.83–5	5.763	5*d*	16.402	2.73–4	4.948
7*s*	16.549	5.05–5	6.766	6*d*	16.573	1.62–4	5.948
8*s*	16.661	3.15–5	7.768	7*d*	16.676	1.04–4	6.947
9*s*	16.732	2.09–5	8.769	8*d*	16.743	7.07–5	7.947
10*s*	16.782	1.46–5	9.769	9*d*	16.788	5.00–5	8.947
11*s*	16.815	1.06–5	10.770	10*d*	16.820	3.67–5	9.947
12*s*	16.841	7.93–6	11.770	11*d*	16.844	2.77–5	10.947
13*s*	16.860	6.09–6	12.771	12*d*	16.863	2.14–5	11.947
14*s*	16.874	4.77–6	13.771	13*d*	16.877	1.68–5	12.947
15*s*	16.886	3.83–6	14.770	14*d*	16.888	1.36–5	13.947
16*s*	16.896	3.06–6	15.773	15*d*	16.897	1.09–5	14.948
17*s*	16.903	2.59–6	16.763	16*d*	16.904	9.22–6	15.942
18*s*	16.910	2.05–6	17.790	17*d*	16.911	7.38–6	16.959
19*s*	16.915	1.85–6	18.739	18*d*	16.916	6.62–6	17.925
$3d\ ^3S^o$	15.385	3.65–4	2.941				
	15.418 [a]	1.09–4 [a]					
	15.420 [b]	1.02–4 [b]					
4*d*	16.087	1.74–4	3.953				
	16.083 [a]	5.58–5 [a]					
	16.080 [b]	5.43–5 [b]					
5*d*	16.404	9.39–5	4.956				
6*d*	16.575	5.59–5	5.958				
7*d*	16.677	3.58–5	6.959				
8*d*	16.743	2.42–5	7.960				
9*d*	16.788	1.71–5	8.960				
10*d*	16.821	1.25–5	9.960				
11*d*	16.845	9.44–6	10.961				
12*d*	16.863	7.29–6	11.961				
13*d*	16.877	5.74–6	12.961				
14*d*	16.888	4.62–6	13.961				
15*d*	16.897	3.72–6	14.962				
16*d*	16.905	3.14–6	15.957				

[a]Taylor and Burke (Ref. [9]).
[b]Henry (Ref. [1]).

race *et al.* and the experiment of Samson and Petrosky at 584 Å. Our result for this ratio shows excellent agreement with the experiment of Dehmer and Dehmer at 304 Å. However, our calculated values are larger than the close-coupling calculation of Pradhan at both wavelengths. Our branching ratio $\sigma(^2P^o)/\sigma(^4S^o)$ is 15–20 % larger than the close-coupling results of Henry at both wavelengths, but agrees very well with the HF calculation of Starace *et al.* Our branching ratio at 584 Å is larger than the close-coupling value of Pradhan, but is smaller at 304 Å. Our calculation is within 15% of the measured value of Samson and Petrosky. Thus, there is an overall good agreement between our calculated values and the experiments at these two wavelengths. The present branching ratio $\sigma(^2P^o)/\sigma(^4S^o)$ is shown by the lower solid curve in Fig. 7.

D. Analysis of autoionizing resonances

We have analyzed the lower members of the autoionizing Rydberg series of resonances below the $^2D^o$, $^2P^o$, and ^4P states of the O^+ ion. The positions E_r, widths Γ_r, and effective quantum numbers n^* are calculated for the $ns\ ^3D^o$ and $nd\ ^3S^o$, $^3D^o$ resonance series converging to the $^2D^o$ threshold, for the $ns\ ^3P^o$ and $nd\ ^3P^o$ series between the $^2D^o$

TABLE V. Resonance parameters of $2s^2 2p^3(^2P^o)ns,nd$ series converging to the $^2P^o$ threshold.

State	E_r (eV)	Γ_r (eV)	n^*	State	E_r (eV)	Γ_r (eV)	n^*
$5s\ ^3P^o$	17.714	3.29–3	4.013	$4d\ ^3P^0$	17.846	1.35–5	
	17.722 [a]	6.48–4 [a]			17.777 [a]	⩽1.00–5 [a]	
	17.69 [b]	3.39–3 [b]			17.77 [b]	1.48–3 [b]	
$6s$	18.017	1.89–3	5.009	$5d$	18.086	1.47–5	5.364
	18.057 [a]	3.04–4 [a]			18.083 [a]	⩽1.00–5 [a]	
	18.04 [b]	1.68–3 [b]			18.08 [b]	7.65–4 [b]	
$7s$	18.182	8.48–5	6.006	$6d$	18.222	1.27–5	6.358
$8s$	18.281	7.50–4	7.004	$7d$	18.307	1.02–5	7.353
$9s$	18.346	5.12–4	8.003	$8d$	18.364	8.03–6	8.349
$10s$	18.391	3.64–4	9.112	$9d$	18.403	6.29–6	9.347
$11s$	18.423	2.68–4	10.001	$10d$	18.432	4.96–6	10.344
$12s$	18.446	2.02–4	11.000	$11d$	18.453	3.95–6	11.343
$13s$	18.464	1.57–4	12.000	$12d$	18.469	3.19–6	12.342
$14s$	18.478	1.23–4	12.999	$13d$	18.482	2.59–6	13.340
$15s$	18.489	9.97–5	13.999	$14d$	18.492	2.15–6	14.340

[a]Taylor and Burke (Ref. [9]).
[b]Henry (Ref. [1]).

and $^2P^o$ thresholds, and $np\ ^3S^o$, $^3P^o$, and $^3D^o$ series converging to the ^4P threshold. The effective quantum number n^* is expressed relative to the assigned thresholds. The diagonalization of the K matrix in the space of open channels N_o gives eigenvalues λ_i that are used to define eigenphase in each channel as

$$\delta_i = \tan^{-1}\lambda_i, \quad i = 1, \ldots, N_o. \tag{2}$$

The eigenphase sum δ is obtained by adding δ_i for all open channels. A resonance position E_r is defined as the energy at which the eigenphase sum δ has maximum value of $d\delta/dE$ and resonance widths are related to the inverse of the eigenphase gradients as described by Quigley and Berrington (QB) [32] in the QB method of resonance analysis using R-matrix theory.

Calculated energies E_r, effective quantum numbers n^*, and widths Γ_r of the autoionizing states of the $ns\ ^3D^o$, $nd\ ^3S^o$, and $^3D^o$ series are listed in Table IV and are compared with available earlier R-matrix calculation of Taylor and Burke [9] and close-coupling calculation of Henry [1]. The $nd\ ^3D^o$ Rydberg series overlaps the $nd\ ^3S^o$ series. The positions agree well with the other calculations, but the present calculated widths are larger. The widths of resonances provide information concerning the interaction between the continuum and Rydberg states. There are no significant perturbations among the various series. The parameters of the resonances of the $ns\ ^3P^o$ and $nd\ ^3P^o$ series converging to the $^2P^o$ ionic threshold are given in Table V. Our results are compared with the earlier R-matrix calculation of Taylor and Burke [9] and close-coupling calculation of Henry [1]. The present resonance positions are shifted to the lower energy for the $ns\ ^3P^o$ series and to the higher energy for the $nd\ ^3P^o$ series compared to earlier calculations.

The resonance parameters of the $np\ ^3S^o$, $^3P^o$, $^3D^o$ series converging to the ^4P threshold are listed in Table VI, where our results are compared with the available calculation of Taylor and Burke [9] and the experiments of van der Meulen *et al.* [23] and Angel and Samson [17]. The positions agree well with the calculation of Taylor and Burke, but the widths of resonances in our calculation are larger; indicating stronger interaction between the Rydberg states and the continua. There is excellent agreement with the experiments of van der Meulen *et al.* and Angel and Samson for the positions and effective quantum numbers of the resonance features. The calculated positions for the lowest three $n=3$ members of the three Rydberg series are slightly shifted to higher-energy side. It may be noted that $n \geqslant 4$ members of the three Rydberg series are very close to each other and these are not resolved in the experiment. The Rydberg series $2s2p^4(^4P)np\ ^3P^o$ is stronger than the other two $np\ ^3S^o$ and $^3D^o$ series. The $np\ ^3S^o$ series follow the $np\ ^3D^o$ series that in turn is followed by the $np\ ^3P^o$ series; in agreement with the experiment. The three Rydberg series do not appear to show any significant perturbation for the lower members ($n \leqslant 14$). However, the higher members ($n \geqslant 15$) almost coincide and perturb each other significantly. We have also detected a very weak $2s2p^4(^4P)nf\ ^3D^o$ series and the parameters of this series are also listed in Table VI.

IV. CONCLUSION

The total and partial photoionization cross sections for the ground $2s^2 2p^4\ ^3P$ state of atomic oxygen in the photon energy range from the $O^+\ ^4S^o$ threshold at 13.62 eV to 60 eV are presented. The cross sections are dominated by Rydberg series of autoionizing resonances converging to various ionic thresholds. A detailed analysis of the resonances converging to the $O^+\ ^2D^o$, $^2P^o$, and ^4P thresholds is performed using the procedure of eigenphase gradients. Our results have been compared with other calculations and experiments. The long-standing discrepancy between theory and experiment for

TABLE VI. Resonance parameters of $2s2p^4(^4P)np,nf$ series converging to the ^4P threshold.

State	E_r (eV)	Γ_r (eV)	n^*	State	E_r (eV)	Γ_r (eV)	n^*
$3p\ ^3S^o$	25.923	1.60–3	2.308	$3p\ ^3P^0$	26.113	4.36–2	2.400
	25.96 [a]	3.34–4 [a]			26.07 [a]	3.57–3 [a]	
	25.84 [c]		2.28 [c]		25.94 [c]		2.33 [c]
	25.88 [b]				25.93 [b]		
$4p$	27.235	5.63–4	3.312	$4p$	27.283	1.60–2	3.377
	27.26 [a]	1.30–4 [a]			27.31 [a]	1.25–3 [a]	
	27.20 [c]		3.30 [c]		27.20 [c]		3.30 [c]
	27.23 [b]				27.23 [b]		
$5p$	27.745	2.77–4	4.313	$5p$	27.765	7.07–3	4.376
	27.76 [a]	6.32–5 [a]			27.78 [a]	5.74–4 [a]	
	27.73 [c]		4.35 [c]		27.73 [c]		4.35 [c]
	27.76 [b]				27.76 [b]		
$6p$	27.994	1.52–4	5.315	$6p$	28.005	3.73–3	5.376
	27.98 [c]		5.40		27.98 [c]		5.40
	28.01 [b]				28.01 [b]		
$7p$	28.135	9.16–5	6.317	$7p$	28.141	2.21–3	6.376
	28.10 [c]		6.30 [c]		28.10 [c]		6.30 [c]
	28.15 [b]				28.15 [b]		
$8p$	28.222	5.91–5	7.318	$8p$	28.226	1.41–3	7.377
$9p$	28.279	4.03–5	8.318	$9p$	28.282	9.60–4	8.377
$10p$	28.319	2.87–5	9.319	$10p$	28.321	6.82–4	9.377
$11p$	28.348	2.11–5	10.319	$11p$	28.349	5.02–4	10.377
$12p$	28.370	1.60–5	11.319	$12p$	28.370	3.80–4	11.377
$13p$	28.386	1.25–5	12.319	$13p$	28.387	2.95–4	12.377
$14p$	28.399	9.83–6	13.320	$14p$	28.400	2.33–4	13.378
$15p$	28.409	7.94–6	14.317	$15p$	28.410	1.87–4	14.375
$16p$	28.418	6.47–6	15.327	$16p$	28.418	1.56–4	15.385
$17p$	28.425	5.29–6	16.299	$17p$	28.425	1.20–4	16.358
$18p$	28.431	4.69–6	17.368	$18p$	28.431	1.23–4	17.417
$19p$	28.435	3.41–6	18.242	$19p$	28.435	6.25–5	18.321
$20p$	28.440	3.91–6	19.436	$20p$	28.440	1.16–4	19.440
$3p\ ^3D^o$	25.830	9.93–3	2.268				
	25.87 [a]	7.13–4 [a]					
	25.75 [c]		2.25 [c]				
	25.79 [b]						
$4p$	27.210	3.35–3	3.278	$4f\ ^3D^0$	27.628	5.12–7	4.006
	27.24 [a]	2.36–4 [a]					
	27.20 [c]		3.30 [c]				
	27.23 [b]						
$5p$	27.734	1.50–3	4.283	$5f$	27.933	4.08–7	5.006
	27.75 [a]	1.06–4 [a]					
	27.73 [c]	4.35 [c]					
	27.76 [b]						
$6p$	27.989	8.02–4	5.286	$6f$	28.099	4.65–7	6.006
	27.98 [c]		5.40 [c]				
	28.01 [b]						
$7p$	28.132	4.77–4	6.288	$7f$	28.199	3.78–7	7.006
	28.10 [c]		6.30 [c]				
	28.15 [b]						
$8p$	28.220	3.06–4	7.289	$8f$	28.263	2.87–7	8.006
$9p$	28.278	2.08–4	8.290	$9f$	28.308	2.16–7	9.006
$10p$	28.318	1.48–4	9.291	$10f$	28.340	1.64–7	10.006
$11p$	28.347	1.09–4	10.291	$11f$	28.363	1.27–7	11.006

TABLE VI. (*Continued*).

State	E_r (eV)	Γ_r (eV)	n^*	State	E_r (eV)	Γ_r (eV)	n^*
12p	28.369	8.22–5	11.291	12f	28.381	9.95–8	12.005
13p	28.386	6.38–5	12.291	13f	28.395	7.93–8	13.006
14p	28.399	5.03–5	13.293	14f	28.406	6.39–8	14.005
15p	28.409	4.06–5	14.290	15f	28.415	5.28–8	15.006
16p	28.418	3.32–5	15.299	16f	28.423	4.26–8	16.005
17p	28.424	2.68–5	16.272	17f	28.429	3.82–8	17.003
18p	28.431	2.44–5	17.339	18f	28.434	2.77–8	18.019
19p	28.435	1.68–5	18.218	19f	28.438	3.01–8	18.976

[a]Taylor and Burke (Ref. [9]).
[b]Angel and Samson (Ref. [17]).
[c]van der Meulen *et al.* (Ref. [22]).

photon energies above the $^2P^o$ threshold has been resolved. Our calculation predicts a broad peak in this energy region that is in agreement with the experiment of Angel and Samson and Samson and Pareek. This peak in our calculation is caused by proper and extensive account of many electron correlation. The peak appears in the partial photoionization cross sections for leaving the O^+ ion in the $^2P^o$ state. Our calculation indicates that the term-dependent correlation effects are more important for the $^2P^o$ state than for the $^4S^o$ and $^2D^o$ states. The large differences with the calculation of Smith for partial photoionization cross sections leaving the ion in the $^2P^o$ state also indicate the importance of electron-correlation effects for the $^2P^o$ state. Electron-correlation effects play an important role in predicting photoionization cross sections near threshold energy regions. The theory and experiment still disagree close to the $^4S^o$ threshold that needs further investigations. Comparison of our partial cross sections with the PES measurement of van der Meulen *et al.* suggests a possible error in normalization of relative measured cross sections; as also argued by Berkowitz [25] on the basis of a sum-rules analysis. We believe that our results are the most extensive and accurate till date and should be useful in the study of atmospheric processes.

ACKNOWLEDGMENT

This research work was supported by NASA.

[1] R. J. W. Henry, J. Chem. Phys. **44**, 4357 (1966).
[2] R. J. W. Henry, Planet. Space Sci. **16**, 1503 (1968).
[3] E. R. Smith, Phys. Rev. A **13**, 1058 (1976).
[4] A. K. Pradhan, J. Phys. B **11**, L729 (1978).
[5] A. K. Pradhan, Planet. Space Sci. **28**, 165 (1980).
[6] G. A. Vesnicheva, G. M. Malyshev, V. F. Orlov, and N. A. Cherepkov, Zh. Tekh. Fiz. **56**, 665 (1985) [Sov. Phys. Tech. Phys. **31**, 402 (1986)].
[7] V. F. Orlov, N. A. Cherepkov, and L. V. Chernysheva, Opt. Spectrosc. (USSR) **64**, 409 (1988) [Opt. Spektrosk. **64**, 683 (1988)].
[8] A. F. Starace, S. T. Manson, and D. J. Kennedy, Phys. Rev. A **9**, 2453 (1974).
[9] K. T. Taylor and P. G. Burke, J. Phys. B **9**, L353 (1976).
[10] K. L. Bell, P. G. Burke, A. Hibbert, and A. E. Kingston, J. Phys. B **22**, 3197 (1989).
[11] C. T. Chen and F. Robicheaux, Phys. Rev. A **50**, 3968 (1994).
[12] R. E. Huffman, J. C. Larrabee, and Y. Tanaka, J. Chem. Phys. **46**, 2213 (1967).
[13] J. L. Kohl, G. P. Lafyatis, H. P. Palenius, and W. H. Parkinson, Phys. Rev. A **18**, 571 (1970).
[14] P. M. Dehmer, J. Berkowitz, and W. A. Chupka, J. Chem. Phys. **59**, 5777 (1973).
[15] P. M. Dehmer, W. L. Lunken, and W. A. Chupka, J. Chem. Phys. **67**, 195 (1977).
[16] J. A. R. Samson and P. N. Pareek, Phys. Rev. A **31**, 1470 (1985).
[17] G. C. Angel and J. A. R. Samson, Phys. Rev. A **38**, 5578 (1988).
[18] M. I. A. Hussein, D. M. P. Holland, K. Coding, P. R. Woodruff, and E. Ishiguro, J. Phys. B **18**, 2827 (1985).
[19] J. L. Dehmer and P. M. Dehmer, J. Chem. Phys. **67**, 1782 (1977).
[20] J. A. R. Samson and V. E. Petrosky, Phys. Rev. A **9**, 2449 (1974).
[21] J. A. R. Samson and W. H. Hancock, Phys. Lett. **61A**, 380 (1975).
[22] P. van der Meulen, C. A. de Lange, M. O. Krause, and D. C. Mancini, Phys. Scr. **41**, 837 (1990).
[23] P. van der Meulen, M. O. Krause, and C. A. de Lange, Phys. Rev. A **43**, 5997 (1991).
[24] W. J. van der Meer, P. van der Meulen, M. Volmer, and C. A. de Lange, Chem. Phys. **126**, 385 (1988).
[25] J. Berkowitz, J. Phys. B **30**, 583 (1997).
[26] M. J. Seaton, in *Recent Studies in Atomic and Molecular*

Processes, edited by A. E. Kingston (Plenum, New York, 1987), p. 29.
[27] S. S. Tayal, J. Phys. B **34**, 2215 (2001).
[28] E. Clementi and C. Roetti, At. Data Nucl. Data Tables **14**, 177 (1974).
[29] A. Hibbert, Comput. Phys. Commun. **9**, 141 (1975).
[30] I. Wenaker, Phys. Scr. **42**, 667 (1990).
[31] K. A. Berrington, W. B. Eissner, and P. H. Norrington, Comput. Phys. Commun. **92**, 290 (1995).
[32] L. Quigley and K. A. Berrington, J. Phys. B **29**, 4529 (1996).